# A Numerical Analysis of Vapor Flow in Concentric Annular Heat Pipes

**A. Nouri-Borujerdi**
e-mail: anouri@sharif.edu

**M. Layeghi**

School of Mechanical Engineering,
Sharif University of Technology,
P.O. Box 11365-9567,
Tehran, Iran

*A numerical method based on the SIMPLE algorithm has been developed for the analysis of vapor flow in a concentric annular heat pipe. The steady-state response of a concentric annular heat pipe to various heat fluxes in the evaporator and condenser sections are studied. The fluid flow and heat transfer in the annular vapor space are simulated using Navier-Stokes equations. The governing equations are solved numerically, using finite volume approach. The vapor pressure and temperature distributions along a concentric annular heat pipe are predicted for a number of symmetric test cases. The vapor flow reversal and transition to turbulence phenomena are also predicted. The results are compared with the available numerical data and have shown good agreement in all cases. Therefore, the vapor flow model developed in this paper has shown good accuracy and convergence behavior in the range of low to moderate radial Reynolds numbers.*
[DOI: 10.1115/1.1760549]

## 1 Introduction

Heat pipes are the most effective passive method of transferring heat available today. Heat pipes can transmit heat at high rates and have a very high thermal conductance. They can transfer heat with low temperature drop and quick response time in a wide range of temperature.

A concentric annular heat pipe (CAHP), as shown in Fig. 1, consists of two concentric pipes of different diameters attached to each other by means of end caps, which create an annular vapor space between the two pipes. Wick structures are placed on both the inner surface of the outer pipe and the outer surface of the inner pipe. There are, however, only a limited number of works concerning the CAHP in the literature. CAHPs are more effective than conventional heat pipes and can be used in many applications including energy conversion systems, cooling of diesel-engine pistons [1], cooling of electronic equipments [2], air conditioning devices, heat recovery systems, furnace applications, high performance space applications, temperature and humidity control, etc.

The vapor flow in heat pipes has been investigated by various authors in the past 40 years. A basic theory was developed by Cotter [3] which has been used since then as a basis for heat pipe design. The flow of vapor was studied in one-dimensional form by Busse [4]. Bankston and Smith [5] modeled the flow of vapor using the stream function and vorticity formulation and determined numerically the pressure and velocity ditributions. Rohani and Tien [6] studied the influence of pressure drop on the temperature distribution in heat pipes using sodium as a working fluid. In their analysis the momentum equations were used in terms of stream function and vorticity coupled with the energy equation in terms of enthalpy. Chi [7], Dunn and Reay [8], and Faghri [9] have published many techniques, theories and applications of different heat pipe structures. Faghri [10] analyzed a two-dimensional, steady and incompressible flow of vapor in a CAHP. A parabolic form of the governing equations of motion was used for the solution of the vapor flow in the evaporator, adiabatic, and condenser sections of the heat pipe. He assumed a zero axial velocity at the evaporator inlet and a fully developed profile at the inlet of the adiabatic and condenser sections. Due to these assumptions, an implicit marching finite difference method is possible. Faghri and Parvani [11] have also studied all features of the laminar vapor flow in a CAHP using a complete two-dimensional incompressible model. Faghri [12,13] also compared various models for vapor flow analysis in the CAHPs. He found that there is no substantial difference between the parabolic and elliptic models but the elliptic model provides more complete simulation of vapor flow than the parabolic model. He experimentally compared the performance characteristics of a copper-water CAHP with a conventional one with the same outer diameter. He reported 80 percent increase in heat transfer for the CAHP case.

In this paper, a numerical method based on an innovative SIMPLE algorithm has been used for the analysis of vapor flow in the CAHPs. Here, the main object is the verification of this innovative SIMPLE algorithm and not dealing with the physics of the operation in annular heat pipes or making some developments in the previous models. The algorithm is developed based on a staggered grid system in order for the study of the dynamics of incompressible vapor flow at low and moderate radial Reynolds numbers in annular heat pipes, for both symmetric and asymmetric heat addition or rejection conditions. Symmetric heat addition and rejection condition is a condition such that all radial Reynolds numbers in the evaporator and condenser sections are the same. Any other condition is considered as an asymmetric condition. QUICK differencing scheme [14] due to its higher accuracy are used for the treatment of convective fluxes, while central differencing scheme is employed for diffusive fluxes. The vapor pressure and temperature distributions along a CAHP are predicted for a number of symmetric and asymmetric test cases. The vapor flow reversal and transition to turbulence are also predicted. The proposed SIMPLE algorithm has shown good convergence behavior at low and moderate radial Reynolds numbers, and even near the transition to turbulence.

## 2 Governing Equations

If we introduce a general variable $\phi$, the conservative form of mass, momentum and energy equations for a laminar steady vapor flow in cylindrical coordinate system can be written in a general form as:

$$\frac{1}{r}\frac{\partial}{\partial r}\left[r\left(\rho v\phi-\Gamma_\phi\frac{\partial\phi}{\partial r}\right)\right]+\frac{\partial}{\partial z}\left[\rho w\phi-\Gamma_\phi\frac{\partial\phi}{\partial z}\right]=S_\phi \quad \text{for} \quad \phi=1,w,v,T \tag{1}$$

where $\Gamma_\phi$ and $S_\phi$ for various conservation equations are given in Table 1.

Contributed by Fluids Engineering Division for publication in the JOURNAL OF FLUIDS ENGINEERING. Manuscript received June 9, 2003; revised manuscript received December 11, 2003. Associate Editor: F. Grinstein.

  

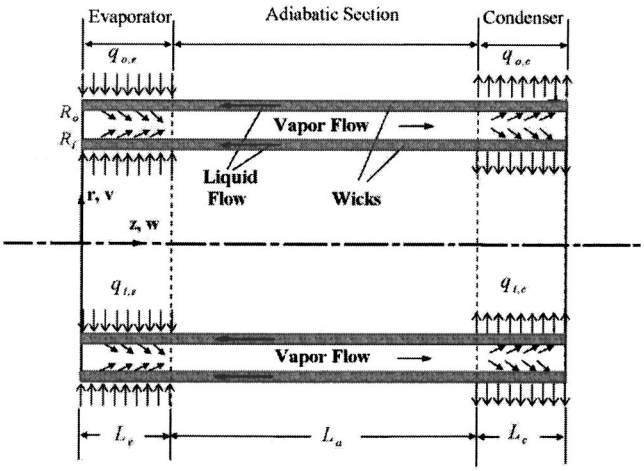


**Fig. 1 Schematic of a CAHP and coordinate system**

$k$ and $C_p$ are thermal conductivity and heat capacity of the vapor at constant pressure respectively. The boundary conditions of the vapor flow in the annular space are defined as follows (Fig. 1).

$$w(0,r)=v(0,r)=0, \tag{2a}$$

$$w(L,r)=v(L,r)=0, \tag{2b}$$

$$w(z,R_i)=w(z,R_o)=0 \tag{2c}$$

$$v(z,R_i)=V_i(z), \tag{2d}$$

$$v(z,R_o)=V_o(z), \tag{2e}$$

$$P(0,r)=0 \tag{2f}$$

if the end caps of the heat pipe are insulated, then

$$\frac{\partial T}{\partial z}(0,r)=\frac{\partial T}{\partial z}(L,r)=0 \tag{2g}$$

where $L=L_e+L_a+L_c$.

The evaporation and condensation are modeled as a uniform injection and suction at the liquid-vapor interface with no phase change assumption.

In this case, the radial blowing and suction velocities at the inner and outer liquid-vapor interface are computed as:

$$V_j(z)=\begin{cases}\pm V_{j,e} & if\ \ 0<z<L_e\\ 0 & if\ \ L_e<z<L_e+L_a\\ \mp V_{j,c} & if\ \ L_e+L_a<z<L\end{cases} \tag{3}$$

$$V_{j,e}=\frac{\dot{q}_{j,e}}{2\pi R_j L_e \rho h_{fg}}, \tag{4a}$$

**Table 1 $\Gamma_\phi$ and $S_\phi$ for various conservation equations**

| Equation | $\phi$ | $\Gamma_\phi$ | $S_\phi$ |
|---|---|---|---|
| continuity | 1 | 0 | 0 |
| z—momentum | $w$ | $\mu$ | $-\frac{\partial p}{\partial z}$ |
| r—momentum | $v$ | $\mu$ | $-\frac{\partial p}{\partial r}-\mu\frac{\partial}{r^2}$ |
| energy | $T$ | $\frac{k}{C_p}$ | $S_T$ |

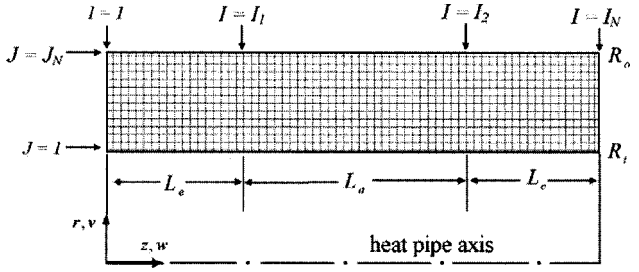


**Fig. 2 Grid arrangement in the vapor flow domain**

$$V_{j,c}=\frac{\dot{q}_{j,c}}{2\pi R_j L_c \rho h_{fg}} \tag{4b}$$

the subscript $j=i, o$ indicates the locations of the prevailing velocities and heat transfer at the inner and outer walls, respectively. $\dot{q}_{j,e}$ and $\dot{q}_{j,c}$ are heat addition to the evaporator and heat rejection from the condenser sections, respectively. $\pm$ signs express the direction of the radial blowing and suction velocities.

The temperature at the vapor-liquid interface of the evaporator and condenser is calculated approximately using Clausius-Clapeyron equation.

$$T_{\text{int}}=\frac{1}{\frac{1}{T_{sat}}-\frac{R}{h_{fg}}\ln\frac{P}{P_{sat}}} \tag{5}$$

$P_{sat}$ and $T_{sat}$ are taken as a reference point and are equal to the condition of the vapor-liquid interface at the end of the evaporator. $R$ is the vapor constant.

## 3 Method of Solution

The governing equations are discretised using a finite volume approach. Only axial symmetric by the annular vapor space is considered in the numerical analysis (Fig. 2). For the numerical analysis a uniform mesh size is used with $40\times80$ cells for the results of Fig. 4 and with $40\times200$ for other figures.

Typical computational cells for a scalar and vector variables are shown in Fig. 3. Node *P* is located at the center of the central cell and nodes *E, W, S and N* are located at the center of the neighboring cells. Nodes *EE, WW, SS and NN* are the neighboring nodes of *E, W, S,* and *N*. To yield a discretized equation at a nodal point *P*, multiplying Eq. (1) by $r$ and integrating over the two-dimensional control volume of the cell *P* gives:

$$\int_w^e\left\{\left[r\left(\rho v\phi-\Gamma_\phi\frac{\partial\phi}{\partial r}\right)\right]_n-\left[r\left(\rho v\phi-\Gamma_\phi\frac{\partial\phi}{\partial r}\right)\right]_s\right\}dz + \int_s^n r\left\{\left[\left(\rho w\phi-\Gamma_\phi\frac{\partial\phi}{\partial z}\right)\right]_e-\left[\left(\rho w\phi-\Gamma_\phi\frac{\partial\phi}{\partial z}\right)\right]_w\right\}dr = \int_w^e\int_s^n rS_\phi dz dr \tag{6}$$

The face values in diffusion and convective terms are discretized by using the central and QUICK differencing schemes [14], respectively. For example, these values for east face of the cell $\rho$ will be

$$\left(\Gamma_\phi\frac{\partial\phi}{\partial z}\right)_e=\Gamma_e\frac{\phi_E-\phi_P}{z_E-z_P} \tag{7}$$

$$F_e\phi_e=\left(\frac{6}{8}\phi_P+\frac{3}{8}\phi_E-\frac{1}{8}\phi_W\right)F_e^+ +\left(\frac{6}{8}\phi_E+\frac{3}{8}\phi_P-\frac{1}{8}\phi_{EE}\right)F_e^- \tag{8}$$

Similar expressions are used for the other faces. Substituting Eqs. (7,8) into Eq. (6), the final generalized discretization equation is as follows.

$$a_P\phi_P=\sum_{nb} a_{nb}\phi_{nb}+b_\phi \tag{9}$$

where the subscript *nb* refers to the neighboring nodes of the node *P*. Finally, the following coefficients are derived.

$$a_E=D_e-\frac{3}{8}F_e^+-\frac{6}{8}F_e^--\frac{1}{8}F_w^-,$$

$$a_W=D_w+\frac{3}{8}F_w^-+\frac{6}{8}F_w^++\frac{1}{8}F_e^+,$$

$$a_N=D_n-\frac{3}{8}F_n^+-\frac{6}{8}F_n^--\frac{1}{8}F_s^-,$$

$$a_S=D_s+\frac{3}{8}F_s^-+\frac{6}{8}F_s^++\frac{1}{8}F_n^+,$$

$$a_{EE}=\frac{1}{8}\overline{F}_e,\quad a_{WW}=-\frac{1}{8}F_w^+$$

$$a_{NN}=\frac{1}{8}\overline{F}_n,\quad a_{SS}=-\frac{1}{8}F_S^+$$

$$a_P=a_E+a_W+a_N+a_s+a_{EE}+a_{WW}+a_{NN}+a_{SS}$$

$$b_\phi=\frac{r_n^2-r_s^2}{2}(z_e-z_w)\overline{S}_\phi$$

where the superscript fluxes $F_k^+$ and $F_k^-$ $(k=n,s,e,w)$ are defined as follows

$$F_k^+=\max(0,F_k), \tag{10a}$$

$$F_k^-=-\max(0,-F_k) \tag{10b}$$

In the above equations, the diffusive and convective terms are defined as follows.

$$D_e=\Gamma_e r_P\frac{r_n-r_s}{z_E-z_P}, \tag{11a}$$

$$D_w=\Gamma_w r_P\frac{r_n-r_s}{z_P-z_W}, \tag{11b}$$

$$D_n=\Gamma_n r_n\frac{z_e-z_w}{r_N-r_P}, \tag{11c}$$

$$D_s=\Gamma_s r_s\frac{z_e-z_w}{r_P-r_S} \tag{11d}$$

$$F_e=\rho r_P(r_n-r_s)w_e, \tag{11e}$$

$$F_w=\rho r_P(r_n-r_s)w_w, \tag{11f}$$

$$F_n=\rho r_n(z_e-z_w)v_n, \tag{11g}$$

$$F_s=\rho r_s(z_e-z_w)v_s \tag{11h}$$

Now we define the correction $\phi'(=w',\ v'$ or $P')$ as the difference between the correct field $\phi\ (=w,\ v$ or $P)$ and the guessed field $\phi^*(=w^*,\ v^*$ or $P^*)$.

$$w_e=w_e^*+d_e(P_P'-P_E'), \tag{12a}$$

$$w_w=w_w^*+d_w(P_W'-P_P') \tag{12b}$$

$$v_n=v_n^*+d_n(P_P'-P_N'), \tag{12c}$$

$$v_s=v_s^*+d_s(P_S'-P_P') \tag{12d}$$

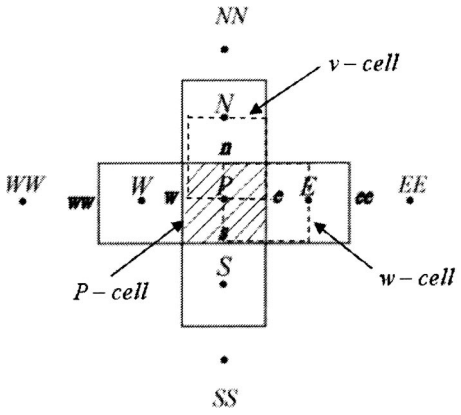


**Fig. 3 Schematic of the computational cells and nodes**

$$P_k=P_k^*+P_k',\quad k=P,N,S,E,W \tag{12e}$$

where

$$d_e=\frac{r_p(r_n-r_s)}{(a_p)_e},\quad d_w=\frac{r_p(r_n-r_s)}{(a_p)_w},$$

$$d_n=\frac{r_n(z_e-z_w)}{(a_p)_n},\quad d_s=\frac{r_s(z_e-z_w)}{(a_p)_s}$$

With a guessed pressure field $P^*$, discretised Eq. (9) for the dashed control volumes around the faces *e*, *w*, *n* or *s* in Fig. 3 yields for example for *e* as:

$$(a_P)_e w_e^*=\sum_{nb} a_{nb}w_{nb}^*+r_p(r_n-r_s)(p_P^*-p_E^*) \tag{13}$$

If we follow the same procedure in Ref. [15], the pressure correction equation is

$$a_{P,P}P_P'=a_{P,E}P_E'+a_{P,W}P_W'+a_{P,N}P_N'+a_{P,S}P_S'+b_P' \tag{14}$$

where $a_{P,E}$, $a_{P,W}$, $a_{P,N}$, $a_{P,S}$, $a_{P,P}$, and $b_P'$ are given by the following equations.

$$a_{P,E}=\frac{\rho[r_p(r_n-r_s)]^2}{(a_P)_e}, \tag{15a}$$

$$a_{P,W}=\frac{\rho[r_p(r_n-r_s)]^2}{(a_P)_w}, \tag{15b}$$

$$a_{P,N}=\frac{\rho[r_n(z_e-z_w)]^2}{(a_P)_n}, \tag{15c}$$

$$a_{P,S}=\frac{\rho[r_s(z_e-z_w)]^2}{(a_P)_s} \tag{15d}$$

$$a_{P,P}=a_{P,E}+a_{P,W}+a_{P,N}+a_{P,S} \tag{15e}$$

$$b_P'=\rho[(z_e-z_w)(r_sv_s^*-r_nv_n^*)+(r_n-r_s)r_p(w_w^*-w_e^*)] \tag{15f}$$

## 4 Solution Procedure

The solution procedure of the discretised equations is based on a line-by-line iteration method in the axial and radial directions using a tri-diagonal matrix solver. The sequence of numerical steps based on SIMPLE algorithm is as follows.

1. Initialize the velocity, pressure, and temperature fields $(w^*,v^*,T^*,P^*)$.
2. Solve Eqs. (9) for $\phi=u$ and *w*.
3. Solve Eq. (14) for $P'$.
4. Correct the velocity and pressure fields by Eqs. (12*a*–*d*).

**Table 2 Design parameters of the CAHP**

| Dimensions (mm) | Fluid Properties |
|---|---|
| $L_e = 200$ | $h_{fg} = 2251.2 \frac{\text{kJ}}{\text{kg}}$ |
| $L_a = 600$ | $C_p = 2.034 \frac{\text{kJ}}{\text{kg K}}$ |
| $L_c = 200$ | $\rho = 0.5974 \frac{\text{kg}}{\text{m}^3}$ |
| | $\mu = 121.00e-7$ Pa.sec |
| $R_o = 23.3$ | $k = 0.0248 \frac{\text{W}}{\text{m.K}}$ |
| $R_i = 14.85$ | $T_{sat} = 373.15$ K |

5. Solve Eq. (9) for $\phi = T$.
6. Check Eq. (16) for convergence, if it is satisfied, calculations will be ended. Otherwise, replace $w^*, v^*, T^*, P^*$ and return to step 2 and repeat the above procedure until convergence is achieved.

The accuracy of the numerical solution is checked first by summation of the absolute value of the relative errors should be equal or less than $10^{-4}$. Second, the spot value should approach a constant value. The relative error, *RE*, in the numerical procedure is defined as:

$$RE = \sum_{cells} \left| \frac{\phi^{n+1} - \phi^n}{\phi^{n+1}} \right|, \quad \phi = w, v, P, T \tag{16}$$

where superscript $n$ refers to the previous iteration.

## 5 Results and Discussion

A computer program has been developed for predicting the velocity, temperature, and pressure fields of vapor along the annular space of a copper-water CAHP. Using this program, various symmetric and asymmetric heat addition and rejection conditions have been analyzed for the design parameters as given in Table 2.

Figs. 4*a–c* show the vapor flow streamlines along the CAHP at low and moderate radial Reynolds numbers ($\text{Re}_r = \rho v_j R_j / \mu$). The radial Reynolds number is based on the radial blowing or suction vapor velocity at the inner or outer vapor walls in the evaporator or condenser section. Also, for a symmetric condition, the radial Reynolds numbers of the evaporator and condenser are the same. The axial velocity profile becomes fully developed in a short distance and stays parabolic all along the length of the heat pipe. In addition, Figs. 4*a–b* show that flow reversal does not occur in the condenser at low radial Reynolds numbers. But this result is not generally correct for all heat pipes. It should be noted that the location where the shear stress becomes zero is called the flow reversal point. Faghri and Parvani [11] have reported that this result is valid only when the condenser zone is short. For the heat pipes with longer condenser lengths, flow reversal may occur for lower radial Reynolds numbers. Experimental prediction of the radial Reynolds number corresponding to the occurrence of flow

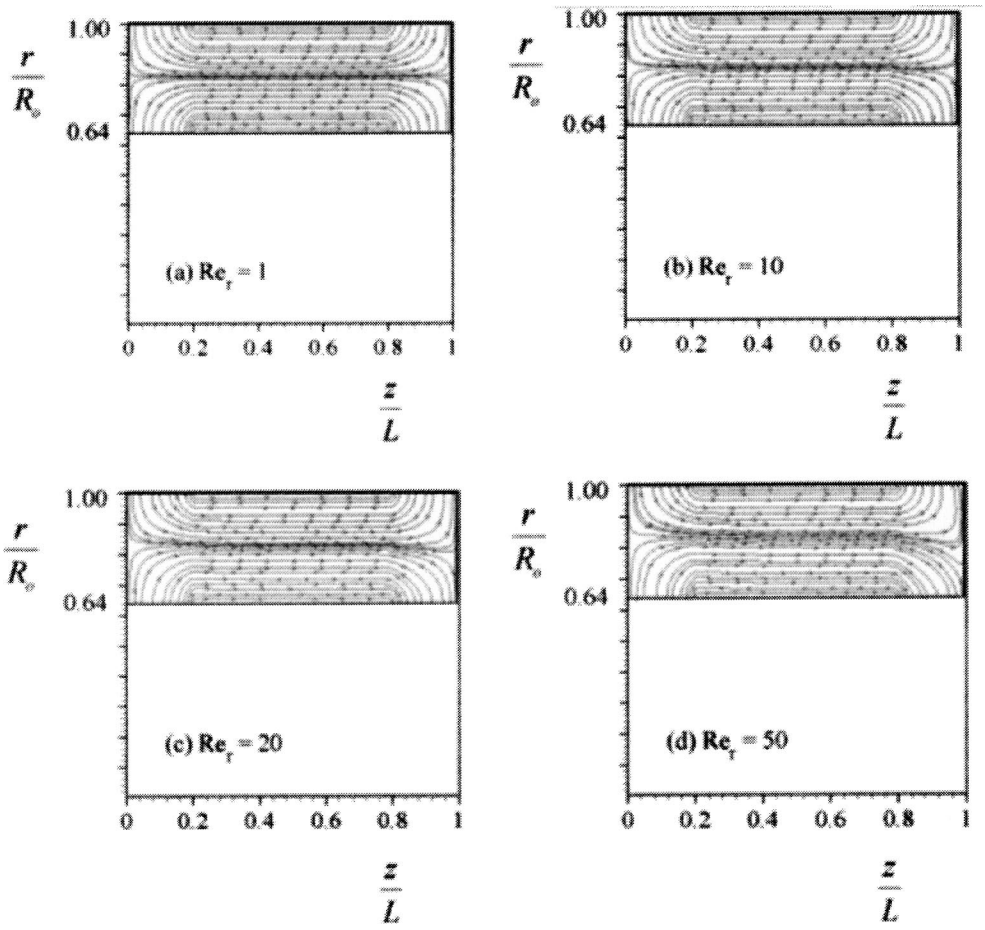


**Fig. 4 Streamlines in the annular space at low to moderate vapor Reynolds numbers**

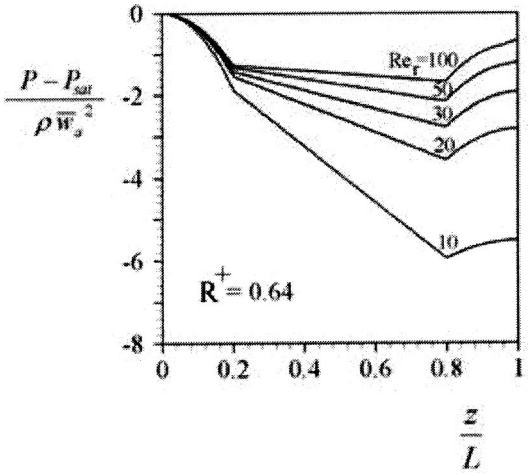


**Fig. 5 Normalized vapor pressure distribution along the annular space centerline**

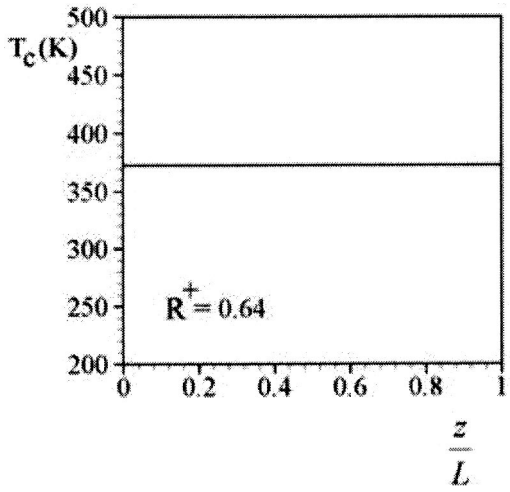


**Fig. 7 Vapor temperature distribution along the annular space centerline**

reversal in a heat pipe is quite complicated. But with the aid of numerical simulation, one can predict the flow reversal condition satisfactorily.

For the heat pipe analyzed here, this condition takes place on the outer pipe wall at radial Reynolds number very close to $Re_r = 19.9$. However, in other situations this condition depends strongly on the length of the condenser section. As the radial Reynolds number increases, the absolute value of the shear stress along the inner and outer wall increases too. The numerical analysis have shown that for the radial Reynolds number $Re_r \approx 19.9$, the shear stress becomes zero at a point very close to the end of the condenser ($z \approx 0.987$m). However, as the radial Reynolds number increases, the flow reversal point moves backward toward the adiabatic section. Under this condition, the reversed flow region extends from the flow reversal point to the end of the condenser. Due to the evaporation and condensation and vapor-liquid interface interactions, the real condition in a heat pipe can be more different from that assumed in the present analysis.

Figure 5 illustrates the pressure distribution along the annular space centerline for various radial Reynolds numbers. It can be seen that as the radial Reynolds number increases, the pressure distributions shift up without considerable change in their overall shapes. As the radial Reynolds number increases the pressure in the condenser section is more recovered. For the pressure drop in the adiabatic section, the present analysis is very close to the fully-developed pressure drop in Hagen-Poiseuille flow. Because pressure decreases linearly along the adiabatic section.

Figures 6a-b depict the normalized pressure distribution along the CAHP for two values of $R^+ = 0.2$ and 0.8 and various radial Reynolds numbers. It is concluded that the present results are in very good agreement with the results presented by Faghri [12]. This demonstrates that the present numerical analysis is sufficiently accurate for predicting the pressure distribution at low and moderate radial Reynolds numbers.

Figure 7 shows the temperature distribution of the annular vapor space centerline. Since the pressure drop along the heat pipe is very small at the low and moderate Reynolds numbers, the present analysis predicts very small temperature drop along the inner and outer walls of the heat pipe (below 0.1°C). This result seems to be logical, as a result of the assumption of thermodynamic equilibrium at the vapor-liquid interface and using Clausius-Clapeyron equation.

**5.1 Transition to Turbulence.** It is assumed that transition to turbulence may take place in the annular space when the axial

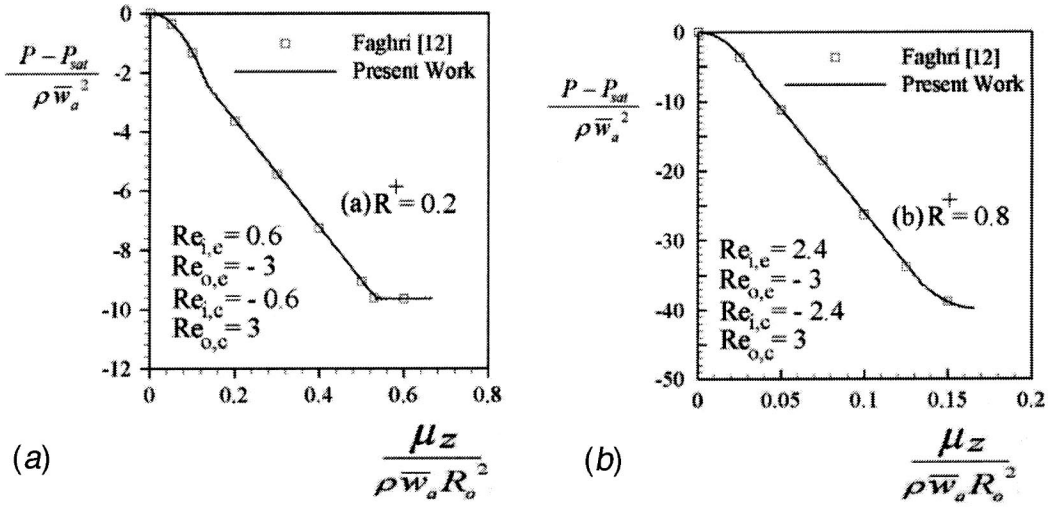


**Fig. 6 Normalized vapor pressure distribution along the CAHP (*a*) low radial Reynolds numbers, (*b*) moderate radial Reynolds numbers**

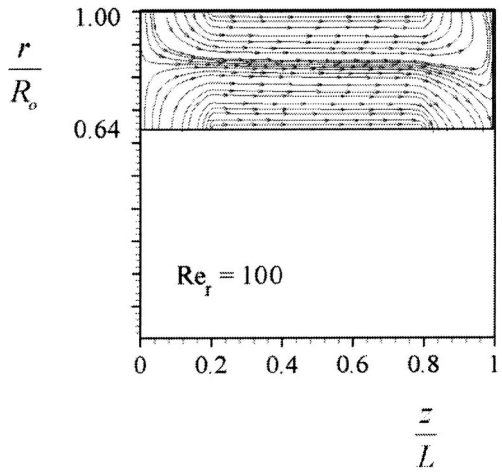


**Fig. 8 Streamline in the annular vapor space**

Reynolds number based on hydraulic diameter $(D_o - D_i)$ and the mean axial velocity $\overline{w_a}$ in the adiabatic section reaches to $\mathrm{Re}_{a,z} = 2300$. Rohani and Tien [6] assumed the value $\mathrm{Re}_{a,z} = 2100$ for a conventional heat pipe. However, this is not generally true for all heat pipes and depends strongly on the flow disturbance and wall conditions. Schlichting [16] has recommended the value 2000 for the transitional Reynolds number, in a non-circular channel. Below this value, the flow seems to be insensitive to the upstream disturbances and always remains laminar. Since the present numerical solution was stable and well-behaved up to, and even above the value 2300, this value is adopted here for the transitional Reynolds number. The axial Reynolds number and the mean axial velocity $\overline{w_a}$ in the adiabatic section can be found as:

$$\mathrm{Re}_{a,z} = \frac{\rho \overline{w}_a D_h}{\mu} = \frac{4L_e}{R_o + R_i}\left(|\mathrm{Re}_{i,e}| + |\mathrm{Re}_{o,e}|\right) \tag{18}$$

$$\overline{w}_a = \frac{\dot{q}_{i,e} + \dot{q}_{o,e}}{\pi \rho (R_o^2 - R_i^2) h_{fg}} \tag{19}$$

For an axial Reynolds number of 2300 and for a symmetric condition, the correpsonding radial Reynolds number of the heat pipe is $\mathrm{Re}_r = 54.8$. Above this value of radial Reynolds number, the laminar flow analysis using a coarse grid may not be valid and accurate prediction of the vapor flow needs experimental work or direct numerical simulation.

Fig. 8 represents the calculated results for $\mathrm{Re}_r = 100$. It is interesting to note that although the radial Reynolds number is higher than the transitional value, $\mathrm{Re}_r = 54.8$, but the numerical results seems to be acceptable and the convergence behavior is also good. The corresponding pressure distribution at $\mathrm{Re}_r = 100$ has been shown in Fig. 5. The large pressure recovery can be seen at the condenser section due to the flow reversal phenomenon. The flow regime seems to be still laminar. Because, the stability limits for laminar flows of this class have not yet been established. However, flows with injection have been found to retain laminar velocity profiles at axial Reynolds numbers greater than $10^5$, as mentioned by Bankston and Smith [5]. This subject should be more studied numerically or experimentally for vapor flow analysis in both conventional and CAHPs. However, at higher radial Reynolds numbers, the flow reversal phenomenon may promote the transition to turbulence and needs to be more studied.

## 5 Conclusion

It has been shown that the incompressible vapor flow and heat transfer in a CAHP can be accurately simulated using the present numerical model. The QUICK differencing scheme has been used in the discretisation process and it has been found that its accuracy is acceptable, at least for moderate radial Reynolds numbers. The proposed SIMPLE algorithm has shown good convergence behavior at low and moderate radial Reynolds numbers and even near the nominal transition to turbulence or higher axial Reynolds number ($\mathrm{Re}_{a,z} = 2300$). It has been also demonstrated that the numerical model works well for the prediction of vapor flow reversal and presents reasonable results even near the transition to turbulence of vapor flow. However, further studies and more complete models are needed to predict these phenomena for a real condition in a CAHP. The presented numerical method was used to analyze the steady-state vapor flow and heat transfer in a CAHP for a number of symmetric and asymmetric heat addition and rejection conditions. The results have been compared with the available numerical data which have been done in the literature and have shown good agreement in all cases. Due to the small pressure drop along the heat pipe at low and moderate radial Reynolds numbers, the present analysis predicts very small vapor temperature drop along the heat pipe.

## Nomenclature

$C_p$ = heat capacity at constant pressure
$D$ = diameter
$h_{fg}$ = latent heat of vaporization
$k$ = thermal conductivity
$L$ = length
$P$ = pressure
$\dot{q}$ = heat transfer
$r$ = radial coordinate
$R$ = gas constant, pipe radius
$R^+$ = radius ratio, $R_i/R_o$
Re = Reynolds number
$S$ = source term
$T$ = temperature
$v$ = radial vapor velocity
$w$ = axial velocity
$z$ = axial coordinate

### Greek Symbols

$\phi$ = general variable
$\mu$ = viscosity
$\rho$ = density

### Subscripts

$a$ = adiabatic, axial
$c$ = condenser, centerline
$e$ = evaporator
$h$ = hydraulic
$i$ = inner wall
int = interface
$o$ = outer
$r$ = radial
$z$ = axial
max = maximum

### Superscripts

$-$ = mean
0 = initial value
$+$ = dimensionless

## References

[1] Wang, Q., Cao, Y., Wang, R., Mignano, F., and Chen, G., 2000, "Studies of a Heat Pipe Cooled Piston Crown," ASME J. Eng. Gas Turbines Power, **122**, pp. 99–105.
[2] Peterson, G. P., 1994, *An Introduction to Heat Pipes: Modeling, Testing, and Applications*, John Wiely, New York.
[3] Cotter, T. P., 1965, *Theory of Heat Pipes*, Los Alamos Scientific Laboratory Report No. LA-3246-MS.
[4] Busse, C. A., 1967, "Pressure Drop in the Vapor Phase of Long Heat Pipes," *Proc. 1967IEEE Thermionic Conversion Specialist Conf.*, Palo Alto, California, p. 391.

[5] Bankston C. A. and Smith H. J., 1971, ''Incompressible Laminar Flow in Cylindrical Heat Pipes,'' *ASME PAPER 17-WA/HT-15*.
[6] Rohani, A. R., and Tien, C. L., 1974, ''Analysis of the Effects of Vapor Pressure Drop on Heat Pipe Performance,'' *International Journal of Heat Mass Transfer*, **17**, pp. 61–67.
[7] Chi, S. W., 1976, *Heat Pipe Theory and Practice*, Hemisphere, Washington, D.C.
[8] Dunn, P. D. and Reay, D. A., 1982, *Heat Pipes*, Pergamon, Oxford.
[9] Faghri, A., 1995, *Heat Pipe Science and Technology*, Taylor & Francis, Washington, D.C.
[10] Faghri, A., 1986, ''Vapor Flow Analysis in a Double-walled Concentric Heat Pipe,'' Numer. Heat Transfer, **10**, pp. 583–595.
[11] Faghri, A., and Parvani, S., 1988, ''Numerical Analysis of Laminar Flow in a Double-walled Annular Heat Pipe,'' J. Thermophys. Heat Transfer, **2**, pp. 165–171.
[12] Faghri, A., 1989, ''Performance Characteristics of a Concentric Annular Heat Pipe Part II-Vapor Flow Analysis,'' ASME J. Heat Transfer, **111**, pp. 851–857.
[13] Faghri, A., and Thomas, S., 1989, ''Performance Characteristics of a Concentric Annular Heat Pipe: Part I-Experimental Prediction and Analysis of the Capillary Limit,'' ASME J. Heat Transfer, **111**, pp. 844–850.
[14] Ferziger, J. H. and M. Peric, 1999, *Computational Methods for Fluid Dynamics*, 2nd ed., Springer-Verlag, Berlin Heidelberg.
[15] Patankar, S. V., 1980, *Numerical Heat Transfer and Fluid Flow*, Hemisphere, New York.
[16] Schlichting, H., 1979, *Boundary Layer Theory*, Mc-Graw-Hill, New York.